Chemical Science

EDGE ARTICLE

View Article Online
View Journal | View Issue

Cite this: *Chem. Sci.*, 2018, **9**, 8221

All publication charges for this article have been paid for by the Royal Society of Chemistry

N-Doped graphene/C_{60} covalent hybrid as a new material for energy harvesting applications†

Myriam Barrejón, ‡[ab] Luis M. Arellano, ‡[a] Habtom B. Gobeze, [c] María J. Gómez-Escalonilla, [a] Jose Luis G. Fierro, [d] Francis D'Souza *[c] and Fernando Langa *[a]

Received 4th May 2018
Accepted 26th August 2018

DOI: 10.1039/c8sc02013b

rsc.li/chemical-science

N-Doped graphene (N-G) was chemically functionalized by *N*-alkylation with the well-known electron acceptor C_{60}. The degree of functionalization and the key structural features of the N-G/C_{60} hybrid were systematically investigated by a number of techniques including thermogravimetric analysis, X-ray photoelectron and Raman spectroscopies and transmission electron and atomic force microscopies. Absorption and electrochemical studies revealed interactions between the N-G and C_{60} while the fluorescence of C_{60} within the hybrid was found to be fully quenched. Evidence for the occurrence of excited state charge transfer from the singlet excited C_{60} to N-G in the hybrid was obtained from femtosecond transient absorption studies covering the visible–near-IR regions. Electron-pooling experiments performed in the presence of a sacrificial electron donor and a second electron acceptor, methyl viologen, revealed the accumulation of the one-electron reduced product of methyl viologen upon continuous irradiation of the N-G/C_{60} nanohybrid, thus revealing the utility of this material in photocatalytic energy harvesting applications.

Introduction

Chemical doping, which has been demonstrated to be operative in carbon nanotubes,[1] is an essential approach to tailor the properties of graphene (G) in order to broaden the applications by creating a band gap.[2] One approach to achieve this goal is substitutional doping by introducing heteroatoms, such as boron, sulfur, phosphorus or nitrogen, into the carbon framework of graphene.[3] In this way, it is possible to modulate the electronic properties of these carbon nanostructures. For example, graphene doped with boron or nitrogen shows p- and n-type semiconducting properties with a shift in the Fermi level below and above the Dirac point, respectively.[4] In particular, N-doped graphene (N-G) has been extensively used in various fields including catalysis,[5–7] electrocatalysis,[8] biosensors,[9] capacitors[10] and field-effect transistors.[11]

When G is doped with nitrogen, three types of N atoms are incorporated into the carbon lattice: pyridine-type N, pyrrole-type N and quaternary N. Both pyridine and pyrrole types are suitable to be functionalized by *N*-alkylation[12] to allow the synthesis of a new family of functionalized G.

The promising field of graphene nanocomposites for energy applications[13] has stimulated the study of supramolecular and covalent hybrids between G or graphene oxide (GO) and donor[14] or acceptor[15,16] organic addends with the aim of promoting photoinduced electron transfer for application in solar cells.[17] However, hybrid materials that take advantage of both the excellent properties of N-G and the electroactive moiety (donor or acceptor) covalently linked to the N atom have not been widely explored.

In the work reported here, we studied the formation of a novel N-G/C_{60} hybrid **4** by *N*-alkylation of N-G with a fullerene derivative; the structural properties of the new hybrid were investigated by thermogravimetric analysis (TGA), X-ray photoelectron (XPS) and Raman spectroscopies, and transmission electron (TEM) and atomic force (AFM) microscopies. In an effort to shed light on the electronic interactions between the two carbon nanostructures, we studied the photophysical properties by absorption and emission spectroscopic techniques including femtosecond transient absorption spectroscopy covering both the visible and near-infrared regions.

Results and discussion

Synthesis and characterization of hybrid N-G/C_{60} 4

Prior to the preparation of the graphene material **4**, the synthesis of fulleropyrrolidine building block **3** was carried out by the widely used approach involving decarboxylation of

[a]*Universidad de Castilla-La Mancha, Instituto de Nanociencia, Nanotecnología y Materiales Moleculares (INAMOL), 45071-Toledo, Spain. E-mail: Fernando.Langa@uclm.es*

[b]*Università degli Studi di Trieste, Dipartimento di Scienze Chimiche e Farmaceutiche, Via Licio Giorgeri, 1 Edifizio C11, 34127 Trieste, Italy*

[c]*Department of Chemistry, University of North Texas, 1155 Union Circle, #305070, 76203-5017, Denton, TX, USA. E-mail: Francis.DSouza@UNT.edu*

[d]*Instituto de Catálisis y Petroleoquímica, CSIC, Cantoblanco, 28049, Madrid, Spain. E-mail: jlgfierro@icp.csic.es*

† Electronic supplementary information (ESI) available: Experimental and synthetic procedures and compound characterization data, along with Fig. S1–S10 and Tables S1 and S2. See DOI: 10.1039/c8sc02013b

‡ These authors contributed equally to this work.

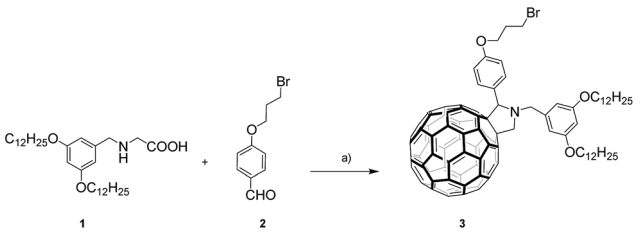

Scheme 1 Synthetic route to fulleropyrrolidine **3**. Reagents and conditions: (a) C_{60}, dry toluene, 3 h, reflux, (32%).

iminium salts obtained by the condensation of *N*-(3,5-didodecyloxybenzyl)glycine **1** [18] and aldehyde **2** [19] (see Scheme 1). Compound **3** was obtained in 32% yield, the structure was confirmed by means of ^{1}H and ^{13}C NMR spectroscopies, and MALDI-TOF MS (see the Experimental section in the ESI†).

The synthesis of the nitrogen-doped graphene–C_{60} nanoensemble, N-G/C_{60} **4**, was performed by *N*-alkylation of pyrrole-type nitrogen atoms onto the graphene surface using potassium carbonate (K_2CO_3) as the base (Scheme 2).[12] For this purpose, commercial nitrogen-doped graphene (http://www.timesnano.com), N-G, was initially exfoliated in *N*-methyl-2-pyrrolidone (NMP)[20] for 15 hours in a sonication bath (37 kHz) at constant temperature (25 °C). The sample was then centrifuged at an appropriate speed to remove the non-exfoliated nitrogen-doped graphene and heavier layers to give predominantly a dispersion of few-layer graphene sheets (3–4 layers) (see further details in the AFM section and ESI†).

N-Alkylation of exfoliated N-G with fulleropyrrolidine **3** was carried out at 150 °C for 4 days in the presence of K_2CO_3 as the base to afford the corresponding N-G/C_{60} hybrid **4**, which was purified by several cycles of sonication, centrifugation and filtration with water, acetone, methanol and dichloromethane to remove all unreacted components (Scheme 2).

The new material was characterized by several complementary techniques in order to confirm that the chemical functionalization of the N-G material had taken place.

The first evidence for the successful covalent functionalization of N-G was obtained from thermogravimetric analysis (TGA).

The TGA plot, measured at 10 °C min^{-1} under nitrogen, of nanoensemble **4** is shown in Fig. S1 (see the ESI†) along with those for fulleropyrrolidine **3** and the starting N-G for the sake of comparison. The thermogram of N-G showed a weight loss of around 10.3% between 300 and 650 °C and this is attributed to defects in the starting material. Nanoensemble **4** displayed an additional weight loss of 33.2% in the first derivative curve in this temperature range, which is directly related to the thermal decomposition maxima of the fulleropyrrolidine **3** units at around 350 °C. These losses matched the desorption in the N-G/C_{60} **4** material.

Raman studies revealed the characteristic D and G bands of graphitic materials at 1356 cm^{-1} and 1590 cm^{-1}, respectively (see Fig. 1). As previously reported for nitrogen-doped graphene,[12] the existence of significant defects related to the presence of nitrogen within the graphitic network increases the intensity of the D band and broadens the Raman bands, thus hampering the observation of any difference after the functionalization process. Evidence for the presence of the C_{60} cage in the new nanohybrid **4** was provided by the peak at 1471 cm^{-1}, assigned to the C_{60} A_g (2) pentagonal pinch mode (Fig. 1a), which is shifted by 11 cm^{-1} compared to the fulleropyrrolidine **3** precursor.[16,21–23] Importantly, in N-G/C_{60} **4** (Fig. 1b) an upshift in the G band due to the p-doping effect[24,25] of C_{60} was observed, as previously reported in the literature for graphene–C_{60} hybrids.[16,23] Finally, a distortion of the 2D band caused by the intercalation of the nitrogen atoms was also observed.[26,27]

FT-IR spectroscopy corroborated the results obtained by the previously described techniques (Fig. S2 in the ESI†). In the spectrum of **4**, the characteristic vibrational modes of C_{60} at 1458, 1164 and 525 cm^{-1} are clearly observed with slight shifts

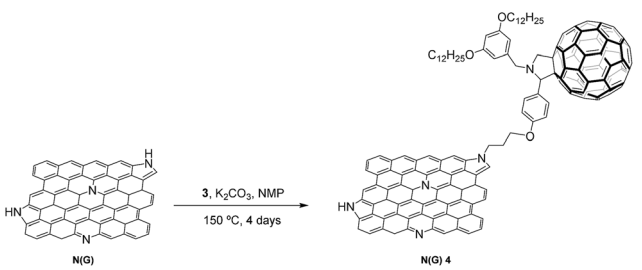

Scheme 2 Preparation of nitrogen-doped graphene nanoensemble N-G/C_{60} **4** by *N*-alkylation.

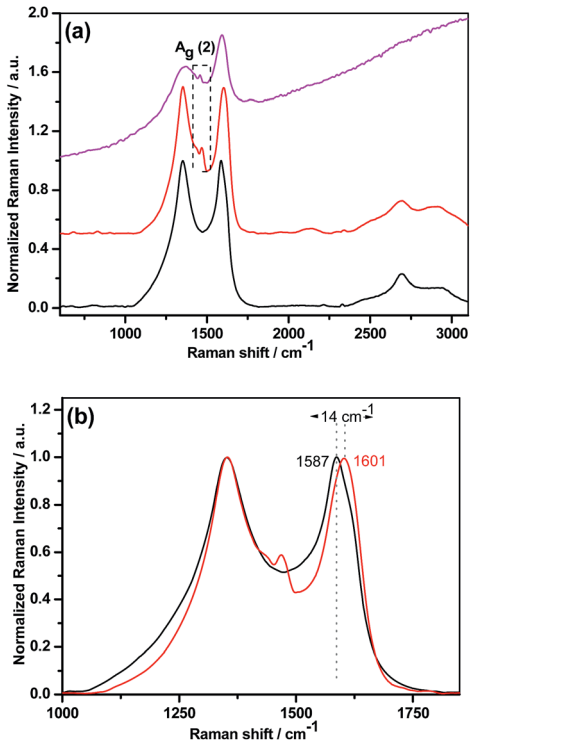

Fig. 1 (a) Raman spectra recorded for N-G (—) compared with N-G/C_{60} **4** (—) and the fulleropyrrolidine precursor **3** (—) excited at 532 nm. (b) Details of the Raman spectra from 1000 to 1850 cm^{-1} for N-G (—) compared with nanoensemble **4** (—). The spectra are normalized to the intensity of the G-mode to facilitate the observation of the peak shift (14 cm^{-1}).

when compared to the precursor **3**, thus suggesting the existence of C_{60} units attached to the hybrid. Interestingly, fulleropyrrolidine **3** presents at 833 cm^{-1} the stretching vibrational mode of the C–Br bond, which disappears after the reaction with N-G, thus confirming that C_{60} units had been covalently bonded to the nitrogen atoms of N-G; in addition, N-G/C_{60} **4** exhibits peaks at around 2950 and 2850 cm^{-1}, assigned to C–H stretching vibrations of alkyl chains,[16,28] along with a strong peak at 1242 cm^{-1} attributed to the asymmetric stretching vibration of Ar–O–C in the ether group.

X-ray photoelectron spectroscopy (XPS) is a surface-sensitive quantitative spectroscopic technique that allows the determination of the elemental composition within a material by giving information about the binding energy, the electronic states and the type of hybridization.[29] A high-resolution N 1s XPS spectrum of the starting nitrogen-doped graphene (N-G) is shown in Fig. S3 and S4 (see the ESI†) and this is deconvoluted into three components located at 398.2, 400.2 eV and 401.8 eV due to pyridinic-N, pyrrolic-N and quaternary nitrogen atoms, respectively[30] (see Fig. S4b in the ESI†). This spectrum contrasts with the single N 1s component observed, as expected, for the bromo-fulleropyrrolidine precursor **3**, with a binding energy of 398.9 eV [23] (see Fig. S6b in the ESI†). After *N*-alkylation, the analysis of the high-resolution N 1s core-level spectrum peak of nanoensemble **4** was satisfactorily fitted to three components (see Fig. 2 and S7 in the ESI†) even though the N 1s component of the anchored fulleropyrrolidine moiety should also be present. However, as the intensity of this peak is expected to be very low, no attempt was made to include this fourth component in the fitting of N 1s emission of nanohybrid **4**. Also, concerning the N 1s component, we observed a shift (~0.3 eV) of the lower binding energies in the XPS N 1s spectrum of the nanohybrid **4** as compared with the N-G material (see Fig. S8 in the ESI†). This shift suggests a charge transfer from nitrogen-doped graphene to fullerene derivative **3**; similar results employing the XPS technique have been obtained for carbon nanotube materials.[31] It should also be noted that the C 1s spectrum of the nanohybrid **4** shows a small contribution at 285.2 eV,[32] which indicates the presence of sp^3 C-atoms of the alkyl chains in fulleropyrrolidine **3** (see Fig. S6a and Table S1 in the ESI†), as observed in previous studies[12,16,28] (Fig. 2).

In addition, the surface composition (atom percentages) was evaluated from peak intensities normalized with atomic sensitivity factors,[33,34] (see Table S2 in the ESI†). It was found that the percentage of nitrogen in N-G/C_{60} **4** decreases with respect to the N-G precursor. This result is expected due to the dilution effect of the C atoms incorporated during the anchoring of the bromo-fulleropyrrolidine moiety. Finally, the absence of bromine in nanohybrid **4** unambiguously confirms the covalent linkage of pyrrolidine[60]fullerene **3** to the N-G material.

Atomic force microscopy (AFM) was used to study the morphology of the final nanoensemble N-G/C_{60} **4** in comparison with the starting N-G. Nitrogen-doped graphene sheets had an average thickness of 3 nm, which corresponds to few-layer graphene (3–4 layer graphene). In addition, the presence of thinner sheets corresponding to single-layer graphene was confirmed in the sample and these had an average height of about 1.4 nm (see ESI, Fig. S9a†). After the *N*-alkylation, the presence of C_{60} aggregates on the new nanoensemble N-G/C_{60} **4** was clearly evidenced by the appearance of brightened zones mainly on the edges of the graphene sheets. N-G/C_{60} **4** displayed step heights ranging from 8 to 24 nm due to the presence of the aforementioned fullerene aggregates (Fig. S9b in the ESI†).

In order to gain further insights into the microstructure of the samples, Transmission Electron Microscopy (TEM) experiments were performed. Suspensions of nitrogen-doped graphene and N-G/C_{60} **4** in ethanol were drop-cast onto a lacey carbon grid and dried under vacuum. The study of nitrogen-doped graphene revealed the presence of stacked thin sheets with folded edges of several hundreds of nanometers in lateral dimensions (Fig. 3). After the functionalization process, a clear change in the morphology was observed due to the presence of C_{60} aggregates on the surface of the graphene sheets. In this case, zoomed images clearly revealed the existence of spherical species with diameters of ~1 nm attached to the edges of the N-G/C_{60} **4** nanoensemble, which are highlighted with red circles in Fig. 3b. It should be noted that, in contrast to these results, isolated C_{60} units were not observable by AFM because of the large uncertainty of this technique during the determination of small structures, which is attributed mainly to the substrate

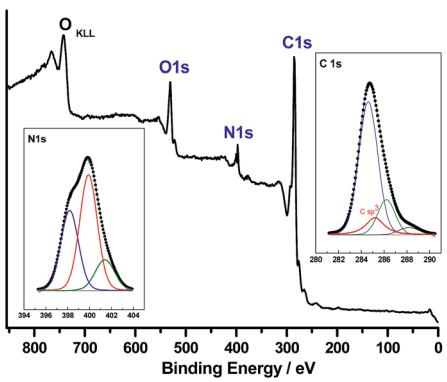

Fig. 2 XPS analysis of N-G/C_{60} hybrid **4**. The insets contain the XPS high-resolution spectra of C 1s and N 1s showing all the components.

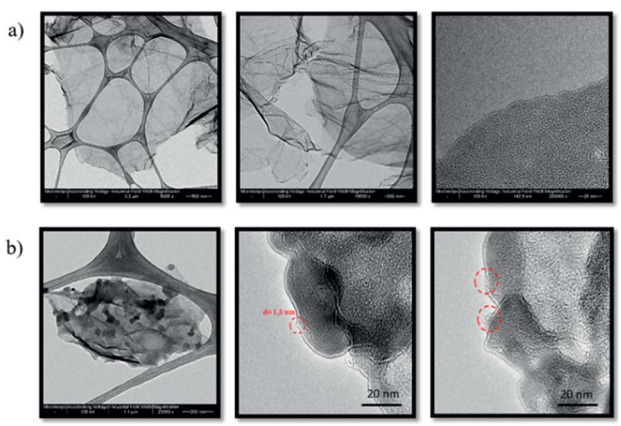

Fig. 3 TEM images of (a) nitrogen-doped graphene and (b) N-G/C_{60} **4** showing spherical C_{60} units highlighted in red circles.

roughness, and the low signal-to-noise ratio.[35–37] In addition, given that the individual C_{60} molecules were mainly present at the outside edge of the graphene sheets, the detection of graphene/C_{60} step heights normally detected in overlapped structures by AFM was not possible in this case.

Further studies on the electronic interaction between fullerene derivative **3** and the nitrogen-doped graphene material were carried out by absorption and fluorescence spectroscopies on samples in *o*-dichlorobenzene (*o*-DCB). The UV-vis absorption spectrum of N-G was almost featureless (Fig. 4a); however, after the functionalization process, a new broad band was observed with a maximum at 416 nm, which is blue-shifted when compared with the characteristic absorption peak of the precursor fullerene derivative **3** (432 nm).

Based on these results, the following conclusions can be drawn: (1) C_{60} units were successfully incorporated onto the graphene surface and, (2) electronic communication exists between the two-electroactive components[16] (fullerene and graphene material).

In order to study the existence of excited-state interactions between the two forms of carbon in the final hybrid, the emission of the materials was studied using isoabsorbent dispersions of nanoensemble **4** and fulleropyrrolidine **3** and using *o*-DCB as solvent (Fig. 4b). Compound **3** exhibits a weak emission band (upon 432 nm excitation) at 711 nm. This band is dramatically quenched (by nearly 81%) in N-G/C_{60} **4** and this suggests the occurrence of excited-state events such as electron transfer or energy transfer.[16]

Electrochemical studies were performed to compare the redox potentials of the nanoensemble **4** and fulleropyrrolidine **3**. The Differential Pulse Voltammograms (DPVs) of the different species in *o*-DCB/acetonitrile solutions containing tetra-*n*-butylammonium hexafluorophosphate ($TBAPF_6$) as the supporting electrolyte are shown in Fig. 5.

In the hybrid N-G/C_{60} **4**, three reduction potentials at −1.18 V, −1.58 V and −2.12 V appeared in the observation window. These potentials are shifted by 30–40 mV with respect to those of fulleropyrrolidine **3** (−1.15 V, −1.54 V and −2.06 V), respectively.

This shift is attributed to the existence of intramolecular electronic interactions in the ground state between the nitrogen-doped material and the fullerene cages, as observed previously in related materials.[16]

Photochemical studies

The steady-state fluorescence studies discussed above revealed quantitative quenching of the fulleropyrrolidine emission in the N-G/C_{60} hybrid **4**, thus suggesting the occurrence of excited state events. This is conceivable since a bandgap of ~0.16 eV exists in N-G due to N-doping.[38] Under such circumstances, the $^1C_{60}^*$ in the N-G/C_{60} hybrid could undergo charge transfer either by donating the electron from the LUMO level of $^1C_{60}^*$ to the valence band of N-G or the half-filled HOMO of $^1C_{60}^*$ could abstract an electron from the conduction band of N-G. The latter charge transfer path is preferred due to the superior electron acceptor behavior of C_{60} (facile reduction); thus, formation of the N-G$^{\bullet+}$–$C_{60}^{\bullet-}$ charge-separated state is expected in the N-G/C_{60} hybrid **4**. In order to provide evidence for such a photochemical event, femtosecond transient absorption studies were performed followed by photocatalytic electron pooling studies,[39,40] wherein the N-G$^{\bullet+}$–$C_{60}^{\bullet-}$ charge separated state generated upon photoexcitation was used to produce the one-electron reduced product of methyl viologen, MV^{2+}. We have successfully used this strategy in the past to demonstrate charge separation and utilization of a charge-separated state in photocatalytic applications in nanocarbon-derived donor–acceptor hybrids.[33,41,42]

The femtosecond transient absorption spectra of pristine N-G dispersed in DMF are shown in Fig. 6a and b and these cover both the visible and near-IR regions. The features of the spectra

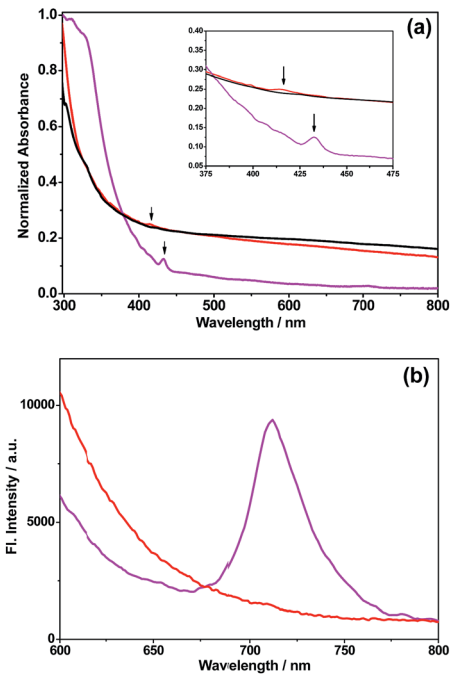

Fig. 4 (a) UV-vis absorption spectrum of N-G/C_{60} **4** (—) compared to the corresponding spectra of N-G (—) and fulleropyrrolidine **3** (—) in *o*-DCB; (b) fluorescence spectrum of N-G/C_{60} **4** (—) compared to that of fulleropyrrolidine **3** (—) in *o*-DCB as the solvent (λ_{exc} = 432 nm).

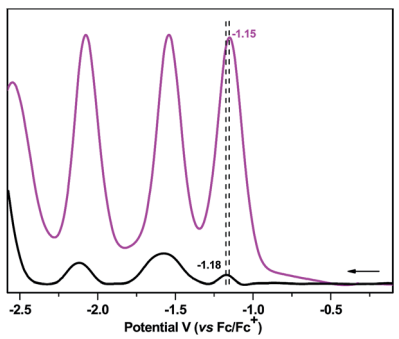

Fig. 5 DPV (reduction run) of fulleropyrrolidine **3** (—) and N-G/C_{60} **4** (—) in *o*-DCB/ACN (4 : 1) containing 0.1 M $TBAPF_6$. Scan rate = 1 mV s^{-1}, pulse width = 0.2 s.

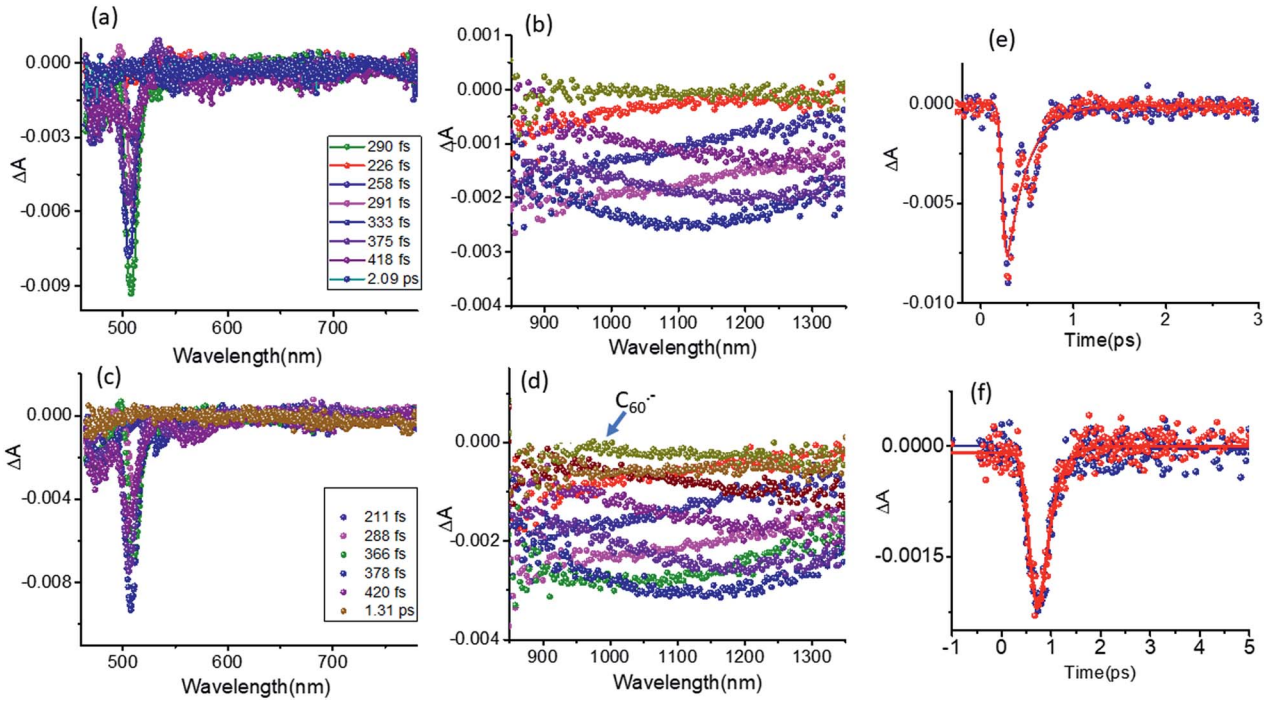

Fig. 6 Femtosecond transient absorption spectra of pristine N-G in the visible (a) and near-IR (b) regions, and of N-G/C_{60} hybrid **4** in the visible (c) and near-IR (d) regions. The samples were excited at 432 nm in DMF. The right-hand panels (e) and (f) show the time profiles of 509 and 1120 nm peaks of pristine N-G (blue) and the N-G/C_{60} hybrid **4** (red).

are largely similar to the transient features of graphene dispersions in organic solvents.[43,44] At the excitation wavelength of 432 nm, the instantaneous formation of optical phonon peaks with peak minima at 506 and 1120 nm was observed. The near-IR signal recovered with a time constant of 1.5 ps. In the case of the N-G/C_{60} hybrid, at the excitation wavelength of 432 nm, where $^1C_{60}^*$ was also expected to form, the spectral features were similar to those of pristine N-G (see Fig. 6c and d). Weak spectral features of $^1C_{60}^*$ in the 850–1000 nm range were largely buried under the strong phonon peaks of N-G (see Fig. S10 in the ESI†) for the femtosecond transient spectra of fulleropyrrolidine. Rapid decay of the $^1C_{60}^*$ signals was also accompanied by weak absorbance in the 1000 nm region, which is attributable to $C_{60}^{\bullet-}$, a product of charge separation. Interestingly, the time profiles for recovery of the visible and near-IR peak were almost identical to that of pristine N-G (see Fig. 6e and f for overlapping time profiles). This suggests that the excited N-G phonons are probably not involved in promoting charge separation but only the $^1C_{60}^*$ is involved in producing the N-G$^{\bullet+}$–$C_{60}^{\bullet-}$ charge-separated state.

As pointed out earlier, the accumulation of electron transfer products using the donor–acceptor hybrids as a photocatalyst not only serves as proof of the occurrence of excited state charge separation in these systems, where it is difficult to characterize spectrally the electron transfer products, but also their usefulness in energy harvesting applications. In the present study, we performed electron pooling experiments involving a sacrificial electron donor, 1-benzyl-1,4-dihydronicotinamide (BNAH), and the electron acceptor methyl viologen (MV^{2+}).[33,42] Direct electron transfer from BNAH to MV^{2+} is an uphill process; however, a charge-separated state from a donor–acceptor hybrid could make this process energetically feasible. Here, continuous irradiation of a mixture of the N-G/C_{60} nanohybrid in the presence of MV^{2+} and BNAH led to the accumulation of $MV^{\bullet+}$ with a characteristic peak at 610 nm (see Fig. 7a inset for solution color before and after the experiment). In the present study, the samples were excited using a xenon lamp with a 400 nm filter to excite selectively the N-G/C_{60} nanohybrid and not the sacrificial electron donor or electron acceptor (BNAH and MV^{2+}) used in the pooling experiment. As shown in Fig. 7a, the addition of more BNAH increased the intensity of $MV^{\bullet+}$ in an experiment involving the N-G/C_{60} nanohybrid. The efficiency of $MV^{\bullet+}$ production with the N-G/C_{60} nanohybrid is shown in Fig. 7b along with the data for pristine N-G and additives alone

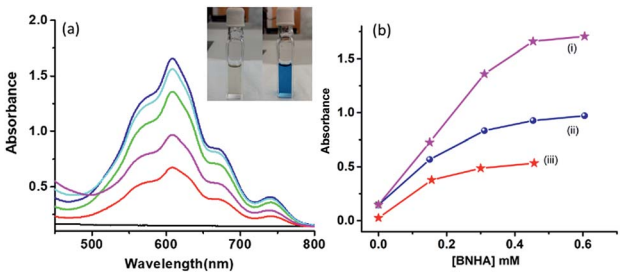

Fig. 7 (a) Electron pooling experiment on the N-G/C_{60} hybrid **4** dissolved in DMF containing 0.5 mM MV^{2+} with the addition of increasing amounts of BNAH. Figure inset shows pictures of the solution before and after the photocatalytic experiment. The blue color is due to the formation of the photocatalytic product $MV^{\bullet+}$. (b) The extent of $MV^{\bullet+}$ formation for (i) N-G/C_{60} hybrid, (ii) N-G and (iii) additives alone.

for the sake of comparison. A higher efficiency was clearly observed when N-G/C_{60} hybrid **4** was used. The results obtained here complement outcomes of a recent study by Jia and co-workers, where N-G/CdS nanocomposites were shown to produce enhanced photocatalytic hydrogen from water under visible light irradiation.[45]

Conclusions

The newly synthesized and characterized N-doped graphene–C_{60} nanohybrid **4** was found to be both electroactive and photoactive, which are useful characteristics for different applications. The synthetic methodology developed here gave reasonable yields of the nanohybrids and it was possible to estimate the degree of functionalization. Ground state interactions between N-G and C_{60} were revealed by absorption and electrochemical studies. Excited state interactions were monitored by fluorescence and femtosecond transient absorption spectral studies. The quenching of C_{60} fluorescence in the N-G/C_{60} hybrids due to excited state charge separation from the $^1C_{60}^*$ state was supported by femtosecond transient absorption studies. The photochemically active N-G/C_{60} hybrid was also found to be a good photocatalyst in an electron pooling experiment, which suggests the usefulness of this system in solar energy harvesting applications.

Compared to pristine graphene derived donor–acceptor hybrids in the literature, the present study involving N-doped graphene stands out in several aspects. Some of these include (i) the N atom in N-G provides a site for facile chemical functionalization, (ii) it would be easier to control the distance between the donor and acceptor, and the type of spacer groups controlling the electronic communication between the entities due to the availability of N sites in the graphene sheet, (iii) as demonstrated in the present study, due to better exfoliation, characterization of mono- or few-layer functionalized NG would be relatively easier, and finally, (iv) control of photochemical events in the donor–acceptor hybrid has been possible to some extent. Further work on functionalized hetero-atom doped graphene derived donor–acceptor hybrids is underway in our laboratories.

Conflicts of interest

There are no conflicts to declare.

Acknowledgements

The Spanish Ministry of Economy and Competitiveness of Spain (CTQ2015-71936-REDT and CTQ2016-79189-R) and the US-National Science Foundation (Grant No. 1401188 to FD) financially supported this research. L. M. A. thanks the Spanish Ministry of Economy and Competitiveness for a doctoral FPI grant. Thanks to Prof. M. Prato for his kind support with the TEM equipment.

Notes and references

1 C. Zhou, J. Kong, E. Yenilmez and H. Da, *Science*, 2000, **290**, 1552.
2 H. Zhang, E. Bekyarova, J.-W. Huang, Z. Zhao, W. Bao, F. Wang, R. C. Haddon and C. N. Lau, *Nano Lett.*, 2011, **11**, 4047.
3 S. Navalón, A. Dhakshinamoorthy, M. Álvaro and H. García, *Chem. Rev.*, 2014, **114**, 6179.
4 L. S. Panchakarla, K. S. Subrahmanyam, S. K. Saha, A. Govindaraj, H. R. Krishnamurthy, U. V. Waghmare and C. N. R. Rao, *Adv. Mater.*, 2009, **21**, 4726.
5 H. Wang, T. Maiyalagan and X. Wang, *ACS Catal.*, 2012, **2**, 781.
6 C. Hua, D. Liub, Y. Xiao and L. Dai, *Prog. Nat. Sci.: Mater. Int.*, 2018, **28**, 121.
7 Y. Cao, S. Mao, M. Li, Y. Chen and Y. Wang, *ACS Catal.*, 2017, **7**, 8090.
8 H. Cui, Z. Zhou and D. Jia, *Mater. Horiz.*, 2017, **4**, 7.
9 H. Fan, Y. Li, D. Wu, H. Ma, K. Mao, D. Fan, B. Du, H. Li and Q. Wei, *Anal. Chim. Acta*, 2012, **711**, 24.
10 H. M. Jeong, J. W. Lee, W. H. Shin, Y. J. Choi, H. J. Shin, J. K. Kang and J. W. Choi, *Nano Lett.*, 2011, **11**, 2472.
11 U. A. Palnitkar, R. V. Kashid, M. A. More, D. S. Joag, L. S. Panchakarla and C. N. R. Rao, *Appl. Phys. Lett.*, 2010, **97**, 063102.
12 M. Barrejón, A. Primo, M. J. Gómez-Escalonilla, J. L. García-Fierro, H. García and F. Langa, *Chem. Commun.*, 2015, **51**, 16916.
13 I. V. Lightcap and P. V. Kamat, *Acc. Chem. Res.*, 2012, **46**, 2235.
14 C. B. KC, S. K. Das, K. Ohkubo, S. Fukuzumi and F. D'Souza, *Chem. Commun.*, 2012, **48**, 11859.
15 L. Wibmer, L. M. O. Lourenço, A. Roth, G. Katsukis, M. G. P. M. S. Neves, J. A. S. Cavaleiro, J. P. C. Tomé, T. Torres and D. M. Guldi, *Nanoscale*, 2015, **7**, 5674.
16 M. Barrejón, M. Vizuete, M. J. Gómez-Escalonilla, J. L. García-Fierro, I. Berlanga, F. Zamora, G. Abellán, P. Atienzar, J.-F. Nierengarten, H. García and F. Langa, *Chem. Commun.*, 2014, **50**, 9053.
17 G. Bottari, M. Á. Herranz, L. Wibmer, M. Volland, L. Rodríguez-Pérez, D. M. Guldi, A. Hirsch, N. Martín, F. D'Souza and T. Torres, *Chem. Soc. Rev.*, 2017, **46**, 4464.
18 F. Ajamaa, T. M. Figueira Duarte, C. Bourgogne, M. Holler, P. W. Fowler and J. F. Nierengarten, *Eur. J. Org. Chem.*, 2005, 3766.
19 E. Shibu, A. Sonoda, Z. Tao, Q. Feng, A. Furube, S. Masuo, L. Wang, N. Tamai, M. Ishikawa and V. Biju, *ACS Nano*, 2012, **6**, 1601.
20 S. P. Ogilvie, M. J. Large, G. Fratta, M. Meloni, R. Canton-Vitoria, N. Tagmatarchis, F. Massuyeau, C. P. Ewels, A. A. K. King and A. B. Dalton, *Sci. Rep.*, 2017, **7**, 16706.
21 M. Vizuete, M. J. Gómez-Escalonilla, J. L. García-Fierro, K. Ohkubo, S. Fukuzumi, M. Yudasaka, S. Iijima, J.-F. Nierengarten and F. Langa, *Chem. Sci.*, 2014, **5**, 2072.
22 X. Zhang, Y. Huang, Y. Wang, Y. Ma, Z. Liu and Y. Chen, *Carbon*, 2008, **47**, 313.
23 M. Barrejón, H. B. Gobeze, M. J. Gómez-Escalonilla, J. L. García-Fierro, M. Zhang, M. Yudasaka, S. Iijima, F. D'Souza and F. Langa, *Nanoscale*, 2016, **8**, 14716.
24 G. Jnawali, Y. Rao, J. H. Beck, N. Petrone, G. Jnawali, Y. Rao, J. H. Beck, N. Petrone, I. Kymissis, J. Hone and T. F. Heinz, *ACS Nano*, 2015, **9**, 7175.

25 D. García, L. Rodríguez-Pérez, M. Á. Herranz, D. Peña, E. Guitián, S. Bailey, Q. Al-Galiby, M. Noori, C. J. Lambert, D. Pérez and N. Martín, *Chem. Commun.*, 2014, **52**, 6677.
26 N. Mahmood, C. Zhang, H. Yin and Y. Hou, *J. Mater. Chem. A*, 2014, **2**, 15.
27 C. Chang, S. Kataria, C. Kuo, A. Ganguly, B. Wang, J. Hwang, K. Huang, W. Yang, S. Wang, C. Chuang, C. Huang, W. Pong, K. Song, S. Chang, J. Guo, Y. Tai, M. Tsujimoto, S. Isoda, C. Chen, L. Chen and K.-H. Chen, *ACS Nano*, 2013, **7**, 133.
28 A. Criado, M. J. Gómez-Escalonilla, J. L. García-Fierro, A. Urbina, D. Peña, E. Guitián and F. Langa, *Chem. Commun.*, 2010, **46**, 7028.
29 M. E. Lipinska, S. L. H. Rebelo, M. F. R. Pereira, J. A. N. F. Gomes, C. Freire and J. L. Figueiredo, *Carbon*, 2012, **50**, 3280.
30 Z. Tian, S. Dai and D. Jiang, *Chem. Mater.*, 2015, **27**, 5775.
31 V. O. Koroteev, L. G. Bulusheva, I. P. Asanov, E. V. Shlyakhova, D. V. Vyalikh and A. V. Okotrub, *J. Phys. Chem. C*, 2011, **115**, 21199.
32 M. Biswal, X. Zhang, D. Schilter, T. K. Lee, D. Y. Hwang, M. Saxena, S. H. Lee, S. Chen, S. K. Kwak, C. W. Bielawski, W. S. Bacsa and R. S. Ruoff, *J. Am. Chem. Soc.*, 2017, **139**, 4202.
33 L. M. Arellano, M. Barrejón, H. B. Gobeze, M. J. Gómez-Escalonilla, J. L. García-Fierro, F. D'Souza and F. Langa, *Nanoscale*, 2017, **9**, 7551.
34 L. M. Arellano, L. Martín-Gomis, H. B. Gobeze, M. Barrejón, D. Molina, M. J. Gómez-Escalonilla, J. L. García-Fierro, M. Zhang, M. Yudasaka, S. Iijima, F. D'Souza, F. Langa and Á. Sastre-Santos, *J. Mater. Chem. C*, 2015, **3**, 10215.
35 P. Nemes-Incze, Z. Osváth, K. Kamarás and L. P. Biró, *Carbon*, 2008, **46**, 1435.
36 C. H. Lui, L. Liu, K. F. Mak, G. W. Flynn and T. F. Heinz, *Nature*, 2009, **462**, 339.
37 A. Mechler, J. Kopniczky, J. Kokavecz, A. Hoel, C.-G. Granqvist and P. Heszler, *Phys. Rev. B: Condens. Matter Mater. Phys.*, 2005, **72**, 125407.
38 C. Zhang, L. Fu, N. Liu, M. Liu, Y. Wang and Z. Liu, *Adv. Mater.*, 2011, **23**, 1020.
39 S. Fukuzumi, H. Imahori, K. Ohkubo, H. Yamada, M. Fujitsuka, O. Ito and D. M. Guldi, *J. Phys. Chem. A*, 2002, **106**, 1903.
40 F. D'Souza, A. S. D. Sandanayaka and O. Ito, *J. Phys. Chem. Lett.*, 2010, **1**, 2586.
41 M. Barrejón, S. Pla, I. Berlanga, M. J. Gómez-Escalonilla, L. Martín-Gomis, J. L. García-Fierro, M. Zhang, M. Yudasaka, S. Iijima, H. B. Gobeze, F. D'Souza, Á. Sastre-Santos and F. Langa, *J. Mater. Chem. C*, 2015, **3**, 4960.
42 L. M. Arellano, L. Martín-Gomis, H. B. Gobeze, D. Molina, C. Hermosa, M. J. Gómez-Escalonilla, J. l. García-Fierro, Á. Sastre-Santos, F. D'Souza and F. Langa, *Nanoscale*, 2018, **10**, 5205.
43 A. Stergiou, H. B. Gobeze, I. D. Petsalakis, S. Zhao, H. Shinohara, F. D'Souza and N. Tagmatarchis, *Nanoscale*, 2015, **7**, 15840.
44 M. E. Ragoussi, J. Malig, G. Katsukis, B. Butz, E. Spiecker, G. de la Torre, T. Torres and D. M. Guldi, *Angew. Chem., Int. Ed.*, 2012, **51**, 6421.
45 L. Jia, D.-H. Wang, Y.-X. Huang, A.-W. Xu and H.-Q. Yu, *J. Phys. Chem. C*, 2011, **115**, 11466.